CHEMISTRY

A European Journal

Accepted Article

Authors: Ashok Yadav, Priyangi Kulkarni, Balu Praveenkumar, Alexander Steiner, and Ramamoorthy Boomi Shankar

WILEY-VCH

COMMUNICATION

WILEY-VCH

Hierarchical Frameworks of Metal-Organic Cages with Axial Ferroelectric Anisotropy**

Ashok Yadav,[a] Priyangi Kulkarni,[c] B. Praveenkumar,*[c] Alexander Steiner*[d] and Ramamoorthy Boomishankar*[a,b]

**Dedicated to Prof. V. Chandrasekhar on the occasion of his 60th Birthday

Abstract: Designing molecular crystals with switchable dipoles for ferroelectric applications is challenging and often serendipitous. Herein, we show a systematic approach toward hierarchical 1D-, 2D- and 3D-frameworks that are assembled via successive linkage of metal-organic cages $[Cu_6(H_2O)_{12}(TPTA)_8]^{12+}$ with chloride ions. Their ferroelectric properties are due to the displacement of channel-bound nitrate counterions and solvated water molecules relative to the framework of cages. Ferroelectric measurements of crystals of discrete and 1D-frameworks assemblies showed axial ferroelectric anisotropy with high remnant polarization. Both, the reversible formation of cage-connected networks and the observation of ferroelectric anisotropic behaviour are rare among metal-ligand cage assemblies.

Ferroelectric materials facilitate large switchable electric fields in low power consumption, non-volatile computing devices, field-effect transistors, electrically controlled magnetic memories, micro-electro-mechanical systems and ferroelectric photovoltaic cells.[1] Ferroelectric systems based on organic, organic-inorganic and metal-organic assemblies have gained attraction due to their simple synthetic protocols, tuneable structural properties and the amenability for low-temperature and low-cost fabrication.[2] Several organic ferroelectrics exhibit polar salt-like structures.[3] The structural aspects of their polarization mechanisms are often well-understood due to the availability of single crystals for X-ray analyses, which can also provide valuable information about axial anisotropies of polarization.[4] In contrast, the polarization of metal-ligand based networks is less well understood owing to the difficulty in growing regular defect-free crystals.[5] Furthermore, their ferroelectric behaviour is often not associated with structure-phase transitions.[6] Known ferroelectric mechanisms in metal-organic assemblies in general involve ordering of the guests and solvates, distortions around the metal centers, motion and distortion of small counter anions

or in some instances the rotational motion of the ligand scaffolds that bridge the metal ions.[7] In here we set out to explore the ferroelectric behaviour of a hierarchical family of metal-organic systems and systematically understand the role of symmetry, dimensionality and guest molecules on their polarization attributes.

Recently, we described a crystalline assembly of cationic metal–organic cages that showed prominent ferroelectric polarization, which originates from the toggling of nitrate anions and solvate molecules found in pockets between the cages.[7f] Here we show that the cationic cage $[\{Cu_6(H_2O)_{12}\}\{TPTA\}_8]^{12+}$ (TPTA = tris(3-pyridylamino)thiophosphate) can be assembled into higher dimensional cage networks. Assemblies of 1D, 2D and 3D-MOFs were obtained by controlled replacement of Cu-bound aqua ligands in the discrete (0D) cage with connecting chloride ions. Further, by using precise quantities of chloride ion acceptors such as $AgNO_3$ or $(^nBu_4N)NO_3$, these networks can be disassembled into the corresponding lower dimensional frameworks in a stepwise manner. The ferroelectric measurements on the crystals of the 0D and 1D assemblies show anisotropic response along the tetragonal a- and c-axes. Interestingly, these measurements show increased remnant polarization of the 1D over the 0D assembly. To the best of our knowledge, this is the first report of a reversible formation of hierarchical cage-connected frameworks with ferroelectric anisotropy in metal-ligand cage assemblies.
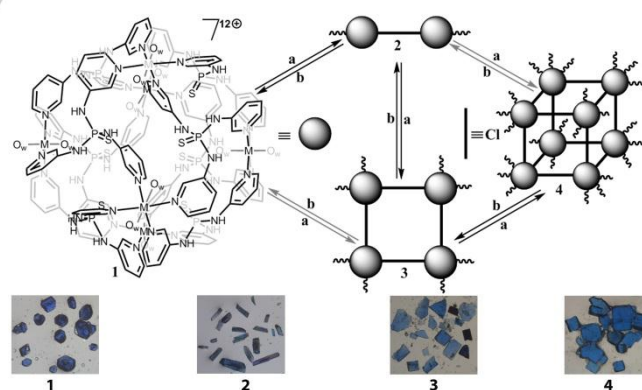

Scheme 1. Schematic diagram for the formation of cage-connected frameworks. Transformations labelled 'a' and 'b' indicate assembly and disassembly processes, respectively. Black arrows show stepwise conversions; gray arrows cross-conversions. Bottom row: Images of the crystals of **1-4** under the microscope.

Treatment of TPTA[7f,8] with $Cu(NO_3)_2\cdot3H_2O$ in 3:2 ratio gave **1**, which contains discrete cages (0D) of formula $\{[Cu_6(H_2O)_{12}][TPTA]_8\}\cdot(NO_3)_{12}\cdot38H_2O$. Reactions of **1** with controlled quantities of NaCl in $MeOH/H_2O$ yielded hierarchical

[a] Dr. A. Yadav and Prof. Dr. R. Boomishankar*, Department of Chemistry, Indian Institute of Science Education and Research (IISER), Pune, Dr. Homi Bhabha Road, Pune – 411008, India.
E-mail: boomi@iiserpune.ac.in
[b] Prof. Dr. R. Boomishankar*, Centre for Energy Science, Indian Institute of Science Education and Research (IISER), Pune, Dr. Homi Bhabha Road, Pune – 411008, India.
[c] P. Kulkarni and Dr. B. Praveenkumar*, PZT Centre, Armament Research and Development Establishment, Dr. Homi Bhabha Road, Pune – 411021, India.
E-mail: praveenkumar@arde.drdo.in
[d] Dr. A Steiner*, Department of Chemistry, University of Liverpool, Crown Street, Liverpool – L69 7ZD, U.K.
E-mail: a.steiner@liverpool.ac.uk
Supporting information for this article is given via a link at the end of the document. CCDC 1584951-1584954 and 1849360-1849364 contains the crystallographic data.

assemblies via sequential replacement of the exo-cage Cu-coordinated water molecules with chloride ions. Thus the 1:1 reaction of **1** with NaCl gave the 1D-polymer $[Cu_6(H_2O)_{10}(TPTA)_8Cl]\cdot(NO_3)_{11}\cdot28H_2O$, **2**; a 1:3 ratio the 2D-network $[Cu_6(H_2O)_7(TPTA)_8Cl_3]\cdot(NO_3)_9\cdot35H_2O$, **3** and a 1:6 ratio (or excess) the 3D-MOF $[Cu_6(H_2O)_6(TPTA)_8Cl_3]\cdot(NO_3)_9\cdot28H_2O$, **4** (Scheme 1). Notably, direct reaction of TPTA, $Cu(NO_3)_2\cdot3H_2O$ and NaCl (in various ratios) only leads to 1D-assembly **2**. The structures of all compounds were determined by single crystal X-ray diffraction (SCXRD), while the bulk phase purity was confirmed by powder X-ray diffraction (PXRD) (Supporting Information, Figures S1-S4). Treatment with chloride ion acceptors such as $AgNO_3$ or $(^nBu_4N)NO_3$ have resulted in the hierarchical disassembly of these frameworks in successive steps from **4** down to **1** (Scheme 1). Although there are a few accounts on the growth of cage assemblies to three dimensional metal organic frameworks, those reactions were not reported to be reversible and complete sets of intermediate frameworks could not be isolated.[9] However, in our case the intermediates were characterized by both SCXRD and bulk phase PXRD (Supporting Information, Figures S5-S8).
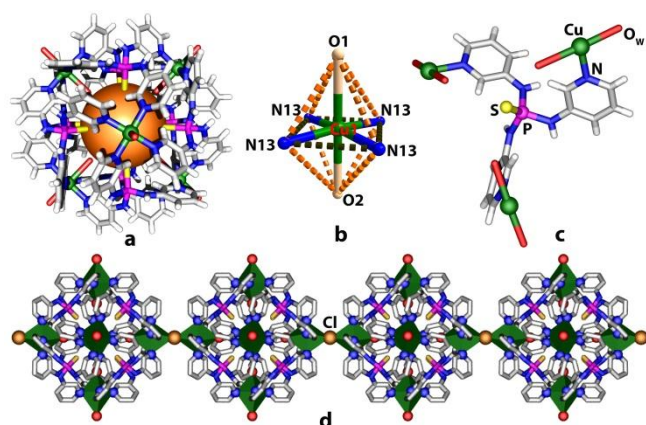
Figure 1. (a) Octahedral core structure of **1** and (b) the coordination at the Cu(II) center. (c) View showing the connection of Cu^{2+} center with the TPTA ligand. (d) View of the cage connected 1D-framework in **2**.

The 0D material **1** crystallized in the tetragonal space group *I*4. It closely resembles the analogous Zn-derivative.[7f] Each TPTA ligand in the cationic $[Cu_6(H_2O)_{12}(TPTA)_8]^{12+}$ cage is connected to three Cu(II) centers via its pyridyl groups. In turn, the Cu(II) ions exhibit characteristic Jahn-Teller-distorted octahedral coordination with four equatorial $N_{pyridyl}$ contacts and two axial water molecules which is well-established in the design of metal-organic cages.[10] The discrete cage is chiral octahedral (point group *O*); the Cu(II) ions occupy the *C* axes, while the TPTA ligands are centred on the C_3 axes (Figure 1a-1c and Supporting Information Figure S9). The cages in **1** are chiral as all tripodal ligands are twisted with the same handedness (Supporting Information, Figures S10).

The SCXRD analyses of **2**, **3** and **4** corroborate the formation of hierarchical cage-connected assemblies. It shows that the exo-cage Cu-bound water molecules have been sequentially

replaced by chloride ions, which act as linear bridges between cages. There are chloride bridges at two opposite corners of the M_6L_8 octahedron in **2** (Figure 1d and Supporting Information, Figures S11)); at its four equatorial corners in **3** and at all six corners in **4**. Non-bridging chloride ions have partially replaced the water molecules at the remaining two corners in **3**. The endo-cage water ligands are unaffected by addition of chloride salt (Figures 2a-b and Supporting Information, Figures S12-S13). Similar discrete and connected cage assemblies were also obtained with other anions such as BF_4^- and ClO_4^- (Supporting Information, Figure S14).

Crystals of **1**, **2** and **3** exhibit tetrahedral lattices with space group symmetries *I*4 (**1**), *I*422 (**2**) and *P*4/nnc (**3**), while **4** gives a cubic lattice (space group *P*432). The topology of the cage network of **3** is a simple square grid (4-c uninodal *sql* net, Figure 2c) considering the cage counts as a single node, while that of **4** is a primitive cubic lattice (6-c uninodal *pcu* net, Figure 2d).[11] All four structures contain large solvent accessible voids, which are occupied by nitrate ions and water molecules.

Remarkably, the handedness of cages is maintained across chloride bridges resulting in chiral networks (Supporting Information, Figures S15-18). A closer look at the crystal structures show that the propeller-shaped $Cu(py)_4$ assemblies at either side of the Cu-Cl-Cu bridge effectively gear into each other in a staggered conformation. The van-der-Waals interactions between pyridyl groups of adjacent cages reinforce the linear arrangement of the Cu-Cl-Cu bridge (Figure S15, Supporting Information). A racemic bridge, on the other hand, would be unfavourable due to the mismatch of opposing shapes. While crystals of **1**, **2** and **4** are chiral throughout, crystals of **3** are centrosymmetric as neighbouring layers form opposite enantiomers.
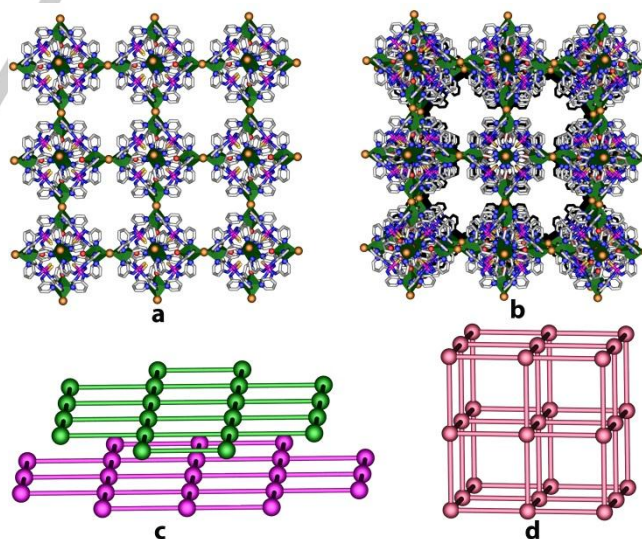
Figure 2. View of the cage connected (a) 2D- sheet in **3** and (b) the 3D-network in **4**. The underlying nets of **3**, showing uni-nodal *sql* topology (c), and **4**, showing uni-nodal *pcu* topology (d).

The cage-connected solids mimic classic inorganic structure types: **2** is related to that of the linear F-bridged polymer BiF_5 (*I*4/m), **3** to the layered structure of SnF_4 (*I*4/mmm), while **4** is analogous to the cubic ReO_3 lattice (*P*m-3m).[12] The lowest packing density is found for the 3D lattice of **4**; its proportion of solvent accessible void volume is 54.1 %. In contrast, the layered lattice of **3** has the highest density with a void volume of 31.5 %, while crystals of **1** and **2** show intermediate values (38.6 % for both). Fig. 3 illustrates the packing of the networks. While the chloride bridges are the primary connections that define the networks, there are additional short contacts between cages of separate networks in the crystal structures of **1**, **2** and **3**. These contacts are facilitated by a nitrate ion that links two tripodal TPTA units via hydrogen bonding. Every cage forms eight such interactions, which bring the separate networks into close contact. Hence, in the case of **3**, the combination of four chloride bridges and eight nitrate contacts yields the densest structure of this series, displaying a near cubic close-packed arrangement. In contrast, the rigid 3D-network of **4** with its six, octahedrally arranged chloride bridges does not feature additional nitrate contacts. The result is a simple cubic packing, which leaves large void spaces.
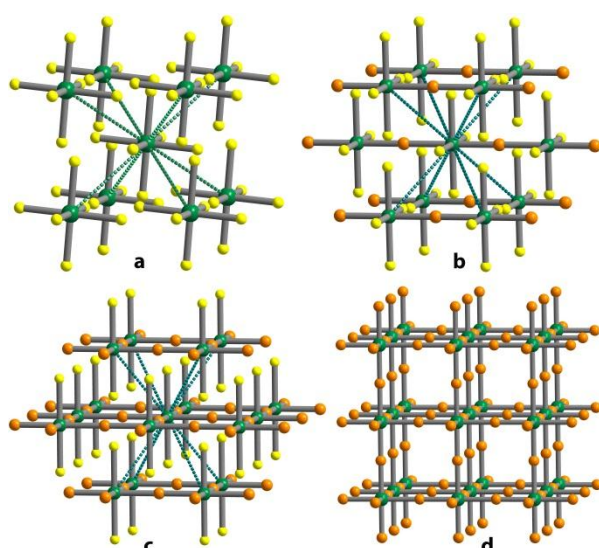
Figure 3. Illustration of the packing of the networks in crystals of **1** (0D, a) , **2** (1D, b) , **3** (2D, c) and **4** (3D, d). Green spheres represent cage-centroids, orange spheres chloride bridges and yellow spheres terminal cage-vertices. Dashed lines show short distances between cages of other networks (< 10 Å when measured between cage-centroids), which are faciliated by hydrogen bonds across nitrate ions.

The dimensionality of the network controls the degrees of freedom that enable the cages to rotate. While the rigid 2D and 3D assemblies prohibit a deviation from a strict orthogonal alignment, the linear chain of **2** should, in principle, permit rotation around its main axis. Indeed, careful examination of the crystal structure of **2** reveals that the cages are rotationally disordered around the crystallographic 4-fold axis which runs along to Cu-Cl-Cu bridges. The rotation angle between the two domains refines to about 5° (Supporting Information, Fig. S11c)

The diffuse character of nitrate ions within the channels of the rigid cage frameworks prompted us to investigate the ferroelectric properties of these crystals. The P-E loop measurements showed that the crystals of **1** and **2** (Supporting Information, Figures S19 and S20) exhibit axial anisotropy giving distinct polarization values along different axes. The loops[13] obtained in the direction of the a-axis gave higher remnant polarization (P_r) values of 20.46 μCcm^{-2} (for **1**) and 28.90 μCcm^{-2} (for **2**) as compared to those obtained along the c-axis (2.0 μCcm^{-2} for **1** and 8.58 μCcm^{-2} for **2**) at 1Hz (Fig. 4). The measurements performed at higher frequencies also gave good P-E loops along the a-axis with P_r values of 5.48 (at 3Hz) and 3.0 μCcm^{-2} (at 5Hz) for **1** while the loops for **2** gave P_r values of 8.75 (at 3Hz) and 5.26 μCcm^{-2} (at 5Hz) (Supporting Information, Figures S21 and S22). The lower coercive fields (E_c) of 1.04 (**1**) and 0.86 (**2**) $kVcm^{-1}$, at 1Hz along a-axis suggest the swift switching of the polarizable domains in both of these crystals. Crystals of **4** gave a circular P-E loop which indicates its non-ferroelectric behaviour (Supporting Information, Figure S23). Crystals of **3** were too small for ferroelectric measurements.
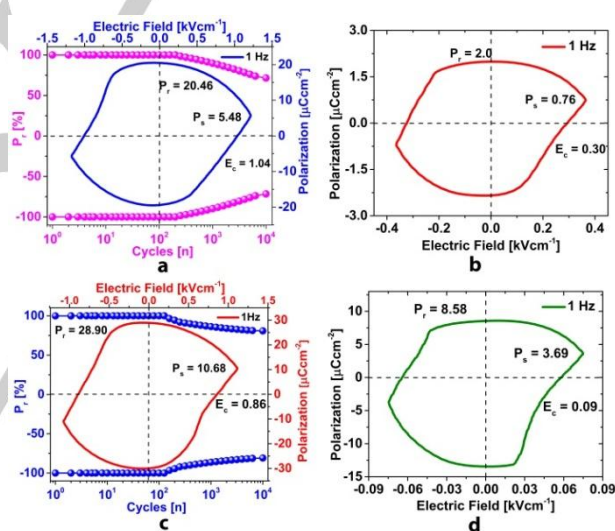
Figure 4. Ferroelctric measurements of **1** (a, b) and **2** (c, d): The figures a and c show the loops along the a-axis and their corresponding fatigue data; b and d are the loops along the c-axis.

The room temperature capacitance measurements on single crystals show higher dielectric constants along the tetragonal a-axis which supports the existence of ferroelectric anisotropy in both **1** and **2** (Supporting Information, Table S2). The plots of current vs. applied voltage gave very low leakage currents along with peaks associated with the domain switching at the coercive fields, typical for ferroelectric materials (Supporting Information, Figures S24 and S25). Furthermore, cycling measurements on **1** and **2** suggests them to be fatigue resistant, as they retain up to 75% of the original P_r after 10^4 switching cycles (Figures 4b and 4d).

The temperature dependence of real part of dielectric permittivity (ε') at various frequencies for **1-4** gave plots with broad anomaly

COMMUNICATION

WILEY-VCH

peaks in the range of 45-50 °C (Figure 5a, Supporting Information, S26-S41). The maximum ε′ values for **1**, **2**, **3**, and **4** corresponding to their peak maxima at 1 kHz were found to be 98.22, 108.91, 67.68 and 60.84, respectively.   Figure 3b illustrates the variations in the ε′ values with respect to the dimensionality of the framework. Notably the higher ε′ values of **1** and **2** over the other frameworks **3** and **4** supports the ferroelectric nature of **1** and **2**. The broad nature of these anomaly peaks can be attributed to the motional dynamics of the loosely bound anions and solvate molecules within the pockets between the cages.[14] The dielectric maxima may be induced by the order-disorder like process of these H-bonded solvates and anions. Further, these anomaly peaks tend to take up relaxer-like behaviour at higher temperatures due to desolvation which is well supported by TGA-DTA, VT-PXRD and FT-IR measurements (Supporting Information, Figure S42-S48).[7c]
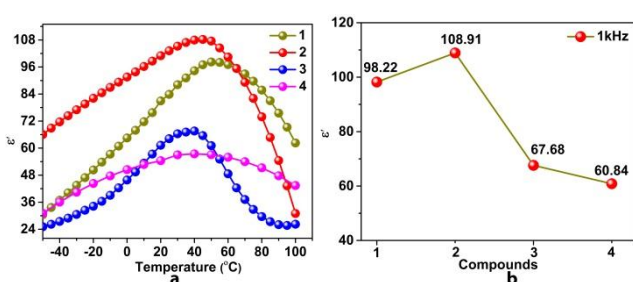
Figure 5. (a) Plots of the real part of dielectric permitivity vs. temperature. (b) Comparison of the dielectric peak maxima in **1**-**4** at 1 KHz.

As stated above, the ferroelectric response in these materials is likely caused by the toggling of diffuse channel bound nitrate ions (Supporting Information, Figures S49-S53). These ions show complex disorder alongside lattice bound water molecules with which they form extended hydrogen bonded networks. The intrinsic cavities of the cages, on the other hand, are void of nitrate ions containing only water molecules. Compound **4** does not show any notable ferroelectric response possibly due to a lower mobility of nitrate ions. They form a spherical net with water molecules close to the cavity walls that may prevent toggling of ions (Supporting Information, Figure S54).

To gain further insights into the anisotropic behaviour, we performed a sequence of experiments on the crystals of **2** where the P-E loops were recorded first along one tetragonal a-axis [1 0 0] and then along the other crystallographically equivalent direction [0 1 0] and then again along [1 0 0]. Surprisingly, we observed a different response along the two directions. For some crystals the first and third readings are strong and the second one is low, while for other crystals the second one is high and the first and third readings are low (Supporting Information, Figure S55), which suggest that there could be some kind of long-range alignment of nitrate ions that is lower in symmetry than tetragonal and has existed prior to the measurements. However, we could not detect evidence of lower symmetry for nitrate ions in the X-ray structures since their contribution to the scattering of the crystal is too low to allow a reasonable refinement in a lower Laue class.The response

along the c-axis [0 0 1], on the other hand, is consistently low (Supporting Information, Figure S56).

In summary, we described a *new* protocol to assemble a discrete metal-organic cage to cage-connected 1D-, 2D- and 3D-networks in a reversible fashion. Treatment of the parent cage assembly of **1** with stoichiometric amounts of chloride ions yields the hierarchical frameworks **2**, **3** and **4** by sequentially replacing the outer-cage axial aqua ligands. Further, these frameworks undergo step-wise disassembly reactions upon treatment with $AgNO_3$ or $(^nBu_4N)NO_3$. The ferroelectric P-E hysteresis loop measurement on the crystals of **1** and **2** show axial anisotropic behaviour for both of them. High remnant polarization (P_r) values of 20.46 and 28.90 µCcm^{-2} were observed along the a-axis for **1** and **2**, respectively, whereas a lower polarization values of 2.0 and 8.58 µCcm^{-2} were obtained for the respective crystals of **1** and **2** along the c-axis. Nevertheless, the tethering of cages into 1D arrangement led to a sizable increase in polarization. The origin of this anisotropic behaviour is due to the toggling of channel-bound nitrate ions with respect to the rigid cage-frameworks. These results promise new synthetic approaches towards metal-ligand assemblies with tunable ferroelectric properties.

[1]   (a) C. A.-P. de Araujo, J. Cuchiaro, L. McMillan, M. Scott, J. Scott, *Nature* **1995**, *374*, 627; (b) S. T. Han, Y. Zhou, V. Roy, *Adv. Mater.* **2013**, *25*, 5425-5449; (c) M. E. Lines, A. M. Glass, *Principles and applications of ferroelectrics and related materials*, Oxford university press, **1977**; (d) G. Rijnders, D. H. Blank, *Nature* **2005**, *433*, 369-370; (e) E. Salje, J. Scott, *Appl. Phys. Lett.* **2014**, *105*, 252904; (f) J. F. Scott, *Science* **2007**, *315*, 954-959; (g) J. F. Scott, *Ferroelectric memories, Vol. 3*, Springer Science & Business Media, **2013**; (h) K. Uchino, *Ferroelectric Devices 2nd Edition*, CRC press, **2009**; (i) T. A. Vanderah, *Science* **2002**, *298*, 1182-1184.

[2]   (a) P. Jain, V. Ramachandran, R. J. Clark, H. D. Zhou, B. H. Toby, N. S. Dalal, H. W. Kroto, A. K. Cheetham, *J. Am. Chem. Soc.* **2009**, *131*, 13625-13627; (b) G. Rogez, N. Viart, M. Drillon, *Angew. Chem. Int. Ed.* **2010**, *49*, 1921-1923; *Angew. Chem.* **2010**, *49*, 1921-1923; (c) A. Stroppa, P. Barone, P. Jain, J. M. Perez-Mato, S. Picozzi, *Adv. Mater.* **2013**, *25*, 2284-2290; (d) A. Stroppa, P. Jain, P. Barone, M. Marsman, J. M. Perez-Mato, A. K. Cheetham, H. W. Kroto, S. Picozzi, *Angew. Chem. Int. Ed.* **2011**, *50*, 5847-5850; *Angew. Chem.* **2011**, *123*, 5969-5972; (e) A. S. Tayi, A. Kaeser, M. Matsumoto, T. Aida, S. I. Stupp, *Nat. Chem.* **2015**, *7*, 281-294; (f) H.-Y. Ye, D.-W. Fu, Y. Zhang, W. Zhang, R.-G. Xiong, S. D. Huang, *J. Am. Chem. Soc.* **2008**, *131*, 42-43; (g) Q. Ye, Y.-M. Song, G.-X. Wang, K. Chen, D.-W. Fu, P. W. Hong Chan, J.-S. Zhu, S. D. Huang, R.-G. Xiong, *J. Am. Chem. Soc.* **2006**, *128*, 6554-6555; (h) W. Zhang, H.-Y. Ye, R.-G. Xiong, *Coord. Chem. Rev.* **2009**, *253*, 2980-2997; (i) Y. Zhang, H. Y. Ye, D. W. Fu, R. G. Xiong, *Angew. Chem. Int. Ed.* **2014**, *53*, 2114-2118; *Angew. Chem.* **2014**, *126*, 2146-2150.

COMMUNICATION

[3]   (a) D. W. Fu, W. Zhang, H. L. Cai, J. Z. Ge, Y. Zhang, R. G. Xiong, *Adv. Mater.* **2011**, *23*, 5658-5662; (b) D.-W. Fu, H.-L. Cai, Y. Liu, Q. Ye, W. Zhang, Y. Zhang, X.-Y. Chen, G. Giovannetti, M. Capone, J. Li, *Science* **2013**, *339*, 425-428; (c) C. Liu, K. Gao, Z. Cui, L. Gao, D.-W. Fu, H.-L. Cai, X. Wu, *J. Phys. Chem. Lett.* **2016**, *7*, 1756-1762; (d) T. Mitsui, *Phys. Rev.***1958**, *111*, 1259; (e) M. Owczarek, K. A. Hujsak, D. P. Ferris, A. Prokofjevs, I. Majerz, P. Szklarz, H. Zhang, A. A. Sarjeant, C. L. Stern, R. Jakubas, S. Hong, V. P. Dravid, J. F. Stoddart, **2016**, *7*, 13108; (f) A. Piecha-Bisiorek, A. Gągor, D. Isakov, P. Zieliński, M. Gałązka, R. Jakubas, *Inorg. Chem. Front.* **2017**, *4*, 553-558.

[4]   (a) J. Harada, T. Shimojo, H. Oyamaguchi, H. Hasegawa, Y. Takahashi, K. Satomi, Y. Suzuki, J. Kawamata, T. Inabe, *Nat. Chem.* **2016**, *8*, 946-952; (b) Q. Pan, Z.-B. Liu, Y.-Y. Tang, P.-F. Li, R.-W. Ma, R.-Y. Wei, Y. Zhang, Y.-M. You, H.-Y. Ye, R.-G. Xiong, *J. Am. Chem. Soc.* **2017**, *139*, 3954-3957; (c) W.-J. Xu, P.-F. Li, Y.-Y. Tang, W.-X. Zhang, R.-G. Xiong, X.-M. Chen, *J. Am. Chem. Soc.* **2017**, *139*, 6369-6375; (d) H.-Y. Ye, J.-Z. Ge, Y.-Y. Tang, P.-F. Li, Y. Zhang, Y.-M. You, R.-G. Xiong, *J. Am. Chem. Soc.* **2016**, *138*, 13175-13178.

[5]   (a) T. Hang, W. Zhang, H.-Y. Ye, R.-G. Xiong, *Chem. Soc. Rev.* **2011**, *40*, 3577-3598; (b) L. Li, J. Ma, C. Song, T. Chen, Z. Sun, S. Wang, J. Luo, M. Hong, *Inorg. Chem.* **2012**, *51*, 2438-2442.

[6]   (a) S. Horiuchi, Y. Tokunaga, G. Giovannetti, S. Picozzi, H. Itoh, R. Shimano, R. Kumai, Y. Tokura, *Nature* **2010**, *463*, 789; (b) A. S. Tayi, A. K. Shveyd, A. C. Sue, J. M. Szarko, B. S. Rolczynski, D. Cao, T. J. Kennedy, A. A. Sarjeant, C. L. Stern, W. F. Paxton, *Nature* **2012**, *488*, 485.

[7]   (a) W. Zhang, H.-Y. Ye, R.-G. Xiong, *Coord. Chem. Rev.* **2009**, *253*, 2980-2997; (b) M. Guo, H.-L. Cai, R.-G. Xiong, *Inorg. Chem. Commun.* **2010**, *13*, 1590-1598; (c) A. K. Srivastava, P. Divya, B. Praveenkumar, R. Boomishankar, *Chem. Mater.* **2015**, *27*, 5222-5229; (d) A. K. Srivastava, B. Praveenkumar, I. K. Mahawar, P. Divya, S. Shalini, R. Boomishankar, *Chem. Mater.* **2014**, *26*, 3811-3817; (e) A. K. Srivastava, T. Vijayakanth, P. Divya, B. Praveenkumar, A. Steiner, R. Boomishankar, *J. Mater. Chem. C* **2017**, *5*, 7352-7359; (f) A. Yadav, A. K. Srivastava, P. Kulkarni, P. Divya, A. Steiner, B. Praveenkumar, R. Boomishankar, *J. Mate. Chem. C* **2017**. *5*, 10624-10629.

[8]   A. Yadav, M. S. Deshmukh, R. Boomishankar, *J. Chem. Sci.*, **2017**, *129*, 1093-1103.

[9]   (a) J.-R. Li, D. J. Timmons, H.-C. Zhou, *J. Am. Chem. Soc.* **2009**, *131*, 6368-6369; (b) S. Wang, T. Zhao, G. Li, L. Wojtas, Q. Huo, M. Eddaoudi, Y. Liu, *J. Am. Chem. Soc.* **2010**, *132*, 18038-18041. (c) J. Canivet, S. Aguado, Y. Schuurman, D. Farrusseng, *J. Am. Chem. Soc.* **2013**, *135*, 4195-4198; (d) D. Enders, M. R. Hüttl, J. Runsink, G. Raabe, B. Wendt, *Angew. Chem. Int. Ed.* **2007**, *46*, 467-469; *Angew. Chem.* **2007**, *46*, 467-469 (e) M. Jahan, Q. Bao, K. P. Loh, *J. Am. Chem. Soc.* **2012**, *134*, 6707-6713; (f) J. Lee, O. K. Farha, J. Roberts, K. A. Scheidt, S. T. Nguyen, J. T. Hupp, *Chem. Soc. Rev.* **2009**, *38*, 1450-1459; (g) H. Li, M. Eddaoudi, M. O'Keeffe, O. M. Yaghi, *nature* **1999**, *402*, 276; (h) M. Pang, A. J. Cairns, Y. Liu, Y. Belmabkhout, H. C. Zeng, M. Eddaoudi, *J. Am. Chem. Soc.* **2013**, *135*, 10234-10237.

[10]   (a) Y. Inokuma , T. Arai, M. Fujita, *Nat. Chem.* **2010**, *2*, 780-783; (b) D. Preston, J. E. M. Lewis, J. D. Crowley, *J. Am. Chem. Soc.* **2017**, *139*, 2379-2386; (c) G. H. Clever, P. Punt, *Acc. Chem. Res.* **2017**, *50*, 2233−2243; (d) G. H. Clever, W. Kawamura, S. Tashiro, M. Shiro, M. Shionoya, *Angew. Chem. Int. Ed.* **2012**, *51*, 2606-2609; (d) K. Byrne, M. Zubair, N. Zhu, X.-P. Zhou, D. S. Fox, H. Zhang, B. Twamley , M. J. Lennox, T. Duŕen, W. Schmitt, *Nat. Commun.* **2017**, *8*, 15268; (e) L. R. Holloway, P. M. Bogie, Y. Lyon, R. R. Julian, R. J. Hooley, *Inorg. Chem.* **2017**, *56*, 11435-11442; (f) D. Luo, X.-Z. Wang, C. Yang, X.-P. Zhou, D. Li, *J. Am. Chem. Soc.* **2018**, *140*, 118-121; (g) C. G. tz, R. Hovorka, G. Schnakenburg, A. Lützen, *Chem. Eur. J.* **2013**, *19*, 10890-10894; (h) N. Struch, C. Bannwarth, T. K. Ronson, Y. Lorenz, B. Mienert, N. Wagner, M. Engeser, E. Bill, R. Puttreddy, K. Rissanen, J. Beck, S. Grimme, J. R. Nitschke, A. Lützen, *Angew. Chem. Int. Ed.* **2017**, *56*, 4930-4935.

[11]   V. Blatov, A. Shevchenko, V. Serezhkin, *J. Appl. Crystallogr.* **2000**, *33*, 1193-1193.

[12]   A. F. Wells, Structural Inorganic Chemistry. Oxford University Press, **2012**.

[13]   (a) S. Horiuchi, Y. Tokura, *Nat. Mater.* **2008**, *7*, 357-366; (b) H. Ma, W. Gao, J. Wang, T. Wu, G. Yuan, J. Liu, Z. Liu, *Adv. Electron. Mater.* **2016**, *2*, 1600038; (c) L. Pan, G. Liu, H. Li, S. Meng, L. Han, J. Shang, B. Chen, A. E. Platero-Prats, W. Lu, X. Zou, *J. Am. Chem. Soc.* **2014**, *136*, 17477-17483.

[14]   (a) H. Cui, B. Zhou, L. S. Long, Y. Okano, H. Kobayashi, A. Kobayashi, *Angew. Chem. Int. Ed.* **2008**, *47*, 3376-3380. (b) H. Cui, Z. M. Wang, K. Takahashi, Y. Okano, H. Kobayashi, A. Kobayashi. *J. Am. Chem. Soc.* **2006**, *128*, 15074-15075. (c) M. Sánchez-Andújar, S. Yáñez-Vilar, B. Pato-Doldán, C. Gómez-Aguirre, S. Castro-García, M. A. Señarís-Rodríguez, *J. Phys. Chem. C*, **2012**, *116*, 13026–13032.

Entry for the Table of Contents

COMMUNICATION

Ferroelectric Anisotropy: A rare family of reversible cage-connected metal-organic assemblies in 1D-, 2D- and 3D-architectures were synthesized from an octahedral $[Cu_6L_8]^{12+}$ cage. The ferroelectric measurements on these assemblies reveal the presence of axial anisotropies in their polarization.
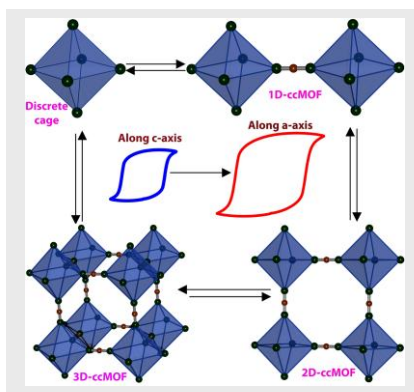
Ashok Yadav, Priyangi Kulkarni, B. Praveenkumar,* Alexander Steiner* and Ramamoorthy Boomishankar*

Page No. – Page No.

Hierarchical Frameworks of Metal-Organic Cages with Axial Ferroelectric Anisotropy

Accepted Manuscript